Relaxation dynamics *vs* crystallization kinetics in the amorphous state: the case of Stiripentol

Guadalupe N. Ruiz,[†,‡] Michela Romanini,[†,‡] María del Barrio,[†,‡] Josep Ll. Tamarit,[†,‡] Luis C. Pardo,[†,‡] and Roberto Macovez[*,†,‡]

Grup de Caracterització de Materials, Departament de Física, Universitat Politècnica de Catalunya, EEBE, Campus Diagonal-Besòs, Av. Eduard Maristany 10-14, E-08019 Barcelona, Spain., and Barcelona Research Center in Multiscale Science and Engineering, Av. Eduard Maristany 10-14, E-08019 Barcelona, Spain.

E-mail: roberto.macovez@upc.edu

Abstract

With the aim of finding a correlation between the crystallization kinetics and the molecular dynamics of a substance that would allow to predict its crystallization time as a function of temperature for a given α relaxation time, we have studied Stiripentol, an anticonvulsant drug. Stiripentol has been characterized in its supercooled liquid, amorphous (glass) and crystalline states by the concurrent use of Broadband Dielectric Spectroscopy (BDS), differential scanning calorimetry, x-ray diffraction and optical microscopy. BDS was employed to study both the dipolar molecular dynamics and the kinetics of crystallization from the melt. Three different molecular relaxation dynamics were identified: an α relaxation corresponding to the collective reorientation of the molecules and associated with the glass transition ($T_g = 246.2 \pm 0.5$ K), a Johari

---

[*]To whom correspondence should be addressed
[†]Grup de Caracterització de Materials
[‡]Barcelona Research Center in Multiscale Science and Engineering

Goldstein β relaxation that can be associated with the single-molecule precursor of the α process, and a γ relaxation arising from intramolecular motions. Isothermal crystallization of Stiripentol was studied by means of BDS well above the glass transition (between 273 K and 293 K) and it was observed under optical microscope at ambient conditions. Stiripentol did not exhibit any sign of polymorphism at ambient pressure, and it recrystallized from the melt into its stable crystalline form. The crystallization kinetics did not obey the Avrami law. Stiripentol displayed a very low nucleation rate, and drops of liquid Stiripentol were observed to crystallize completely from a single nucleus before the appearance of new nuclei, so that the crystallite grew according to the morphology of the liquid domains, a fact that might explain the lack of validity of the Avrami law. Possible correlations between the crystallization kinetics and the molecular dynamics have been analyzed, finding that the crystallization time has a sublinear dependence on the cooperative relaxation time, as is the case in other substances reported in the scientific literature. This could suggest a general correlation of these parameters, at least at temperatures above T_g. The low nucleation rate is an interesting feature in the quest of possible mechanisms that allow enhancing the physical stability of amorphous drugs.

Keywords

Anticonvulsant drug, amorphous formulations, physical stability, molecular mobility, crystal growth, dielectric spectroscopy

Introduction

Active pharmaceutical ingredients (API's) are generally stored in solid form, either as crystalline or amorphous (glassy) powders.[1–3] The amorphous form of API's, though being thermodynamically unstable,[4,5] offers some advantages: amorphous phases show more solubility and better dissolution profiles and hence better bioavailability than crystal phases, by virtue

of their higher free energy.[6–9] It has also been reported that in some cases amorphous drugs can be compacted into tablets more effectively than polycrystalline powders, even omitting the addition of excipients.[10] By means of formulation in amorphous phase, many drugs with originally poor aqueous solubility have reached the drug development stage during the last decade.[11–13] Although the detailed microscopic mechanisms governing the kinetic stability of amorphous API's remain unknown, the crystallization kinetics appears to be determined by a large number of factors such as preparation method, thermal and mechanical treatments employed during formulation, storage temperature, application of pressure, or exposure to humidity.[14,15] It is then of utter importance to find out which are the mechanisms taking place in the amorphous to crystalline transformation, so as to be able to find optimum production and storage conditions of the formulated drug.[16–22]

Many factors are involved in the stability of a substance. Thermodynamic quantities such as differences in free energy between the phases involved and interfacial energies, play a role as they determine the stable phase of the system and the energetic cost of having a mixed-phase sample. However, thermodynamic quantities mostly reflect equilibrium behavior, and only to a smaller extent the kinetics to reach the equilibrium state. It is well-known that there are two main relevant factors for the recrystallization process, thermodynamics and kinetics.[23] In this respect, it is interesting to note that a recent review indeed suggested that the molecular mobility (rather than thermodynamic quantities) appears to be the most important factor governing the crystallization rate.[24] It is also recognized that the complexity of the problem makes difficult, at present, the establishment of clear correlations between molecular mobility and physical stability, mainly due to the complexity of the involved molecular entities and their inter- and intramolecular interactions as well as due to the different time scales involved in amorphous materials, not only the so-called 'global mobility' which refers to the structural relaxation (α-relaxation). As for the thermodinamical aspect of recrystallization, lowering the temperature of the supercooled liquid decreases the steady state nucleation and growth rates, but, according to the kinetics, it increases the liquid's viscosity which is responsible for

3

delaying the recrystallization.[24] The problem is even more difficult because nucleation and growth are commonly simultaneous effects that cannot be set apart. The case of Stiripentol is an unusual and outstanding case because nucleation is unlikely and only growth plays a role within the recrystallization process.

Stiripentol (STP; 1-(1,3-benzodioxol-5-yl)-4,4-dimethyl-1-penten-3-ol, $C_{14}H_{18}O_3$) is an anti-convulsant drug, structurally unrelated to the currently available antiepileptics.[25] It is used for the treatment of Dravet syndrome or severe myoclonic epilepsy in infancy (SMEI) in conjunction with sodium valporate and clobazam when seizures are not adequately controlled with the association of these two medications.[26,27] STP is practically insoluble in water and aqueous fluids,[28,29] and hence it is commercialized in the form of gelatin capsules or in the form of granules for a drinkable suspension (Diacomit®). The state of the art in STP research is of great impact and relevance. Around 1% of the world's population suffer from epilepsy of different types, among which one third still don't have effective anti-epileptic drugs clinically available. It has been recently reported that STP is an LDH inhibitor that suppresses neural activity and seizures, and is in fact the first antiepileptic drug that acts on metabolic pathways, mimicking the effect of ketogenic diets used in drug-resistant epilepsy.[30] Given the low solubility of STP in water, it might be interesting if its amorphous phase could be stabilized to improve its dissolution rate in the body and hence its bioavailability, while avoiding crystallization. In this contribution, we study the molecular dynamics and isothermal crystallization of STP, and analyze the possible correlation between the crystallization time and the characteristic time of molecular relaxations. Despite the fact that the crystallization kinetics does not follow the Avrami law, we find the same sublinear correlations between the cooperative relaxation time and the crystallization time observed in other amorphous drugs.[31–34] Finding a correlation model between these magnitudes would be of great interest since it would help predicting the crystallization kinetics of a substance at different temperatures, enabling the development of stabilization protocol approaches.

Experimental section

STP was acquired from Biocodex Laboratoire with purity higher than 99%. Differential scanning calorimetry experiments by means of a Q100 from TA Instruments were done by melting, cooling and reheating STP samples inside an aluminum capsule. Measurements were performed in the temperature range from 203 K to 393 K, with a heating/cooling rate of 2 K/min with masses arounf 10 mg and under nitrogen atmosphere.

A *Novocontrol Alpha analyzer* was used for Broadband Dielectric Spectroscopy (BDS) measurements. The sample was placed in a stainless steel parallel-plate capacitor specially designed for the analysis of liquids, with the two electrodes kept at fixed distance by means of silica spacers of 50 μm diameter. Temperature control of the capacitor and thus of the sample was achieved with a nitrogen-gas flow cryostat with an error not higher than 0.3 K. Two different BDS experiments were carried out, in order to study the relaxation dynamics and the crystallization kinetics of the material. In the former case, the sample in crystalline state was placed in the capacitor, melted at 373.2 K, and quenched to 120 K inside cryostat. Successive isothermal measurements were done every 2 K, from 180 K to 296 K in the frequency (f) range between 10^{-2} Hz to 10^6 Hz. STP exhibited three dynamic processes, namely a collective primary relaxation at lower frequency (α process),a secondary dynamics at higher frequency (β process) and a γ relaxation arising from intramolecular motions. The acquired dielectric loss spectra were analyzed by fitting the loss features with Havrilak-Negami (HN) functions. A background proportional to reciprocal frequency was added to model the conductivity contribution to the loss spectra. The analytic expression of the HN function without the conductivity contribution is:[35,36]

$$\epsilon_{HN}(f) = \epsilon_\infty + \frac{\Delta\epsilon}{(1 + (i2f\tau_{HN})^a)^b} \tag{1}$$

where $\Delta\epsilon = \epsilon_s - \epsilon_\infty$ is the dielectric strength (equal to the step variation of ϵ', and proportional to the density of the molecules taking part in the relaxation process), and

ϵ_∞ and ϵ_s are the high-frequency and static low-frequency limits of the real permittivity. The HN exponents, a and b are related to the shape and symmetry of the relaxation time distribution, and lie within 0 and 1. The characteristic time τ at which the dielectric loss of each relaxation is maximum was obtained from the corresponding τ_{HN} value and HN exponents according to:

$$\tau = \tau_{HN} \left(sin \left(\frac{a\pi}{2 + 2b} \right) \right)^{-1/a} \left(sin \left(\frac{ab\pi}{2 + 2b} \right) \right)^{1/a} \tag{2}$$

A special case of the HN function (*Eq. (1)*) is the *Cole-Cole* function, which corresponds to the case that the symmetry parameter b is equal to 1, leading to symmetric relaxation peaks.

The second BDS experiment, designed to study the isothermal crystallization kinetics of STP, consisted in measuring the decrease of strength of the dielectric loss as a function of time during the crystallization of the supercooled material at different fixed temperatures. To this end, the molten sample was placed inside a precooled cryostat at 233 K (about 13 K below T_g) and then the temperature was raised at a rate of 10 K/min until reaching the desired temperature of the experiment, (T_e). We measured the recrystallization at five different T_e temperatures between 273 and 293 K in the frequency range from 10^2 to $10^6 Hz$. These dielectric measurements were carried out on the same sample, which was re-melted and re-vitrified prior to each experimental run.

In order to discard the existence of a possible polymorphism of STP at ambient pressure, high-resolution X-ray powder diffraction data were recorded. A horizontally mounted INEL cylindrical position-sensitive detector (CPS-120) with a Debye-Scherrer geometry was used, with angular step of ca. $0.029° - 2\theta$ over a 2θ-range from 2 to 60°. The system works with monochromatic $CuK\alpha_1$ radiation ($\lambda = 1.5406$, 40 kV and 25 mA) and is equipped with a liquid nitrogen 700 series Cryostream Cooler from Oxford Cryosystems (accuracy of 0.1 K). STP samples were loaded at ambient conditions into a 0.5-mm-diameter Lindemann capillar, which could rotate around its axis during data collection in order to minimize the effect of

preferential orientation. Three samples were measured: the as-provided crystalline powder (as received from the manufacturer), the supercooled liquid during the crystallization process, and a fully recrystallized sample. The first and last were measured at ambient temperature (300 K), while the second was studied at 273 K.

Results and discussion

Relaxation Dynamics

Fig. 1 shows the loss spectra, i.e imaginary part of the complex relative dielectric permittivity, of STP in its supercooled liquid state and glass state, as measured upon heating from low temperature (only some measurements from 140 K to 282 K are shown, for clarity). The molecular structure of STP is shown in the inset of panel *(b)*. A primary relaxation is observed, visible as an asymmetric peak in the loss spectra of *Fig. 1(a)*. This relaxation corresponds to the collective reorientation of the STP molecules, as will be shown later. Upon decreasing the temperature, this feature shifts to lower frequency. At low-temperature a second relaxation (β process) is observed, indicated by the arrow at the bottom of panel *a* and in the middle of panel *b*. Finally, for temperatures lower than 240 K, another relaxation (γ) can be observed, as marked in panel *(b)*. The two latter relaxations were fitted with *Cole-Cole* functions.
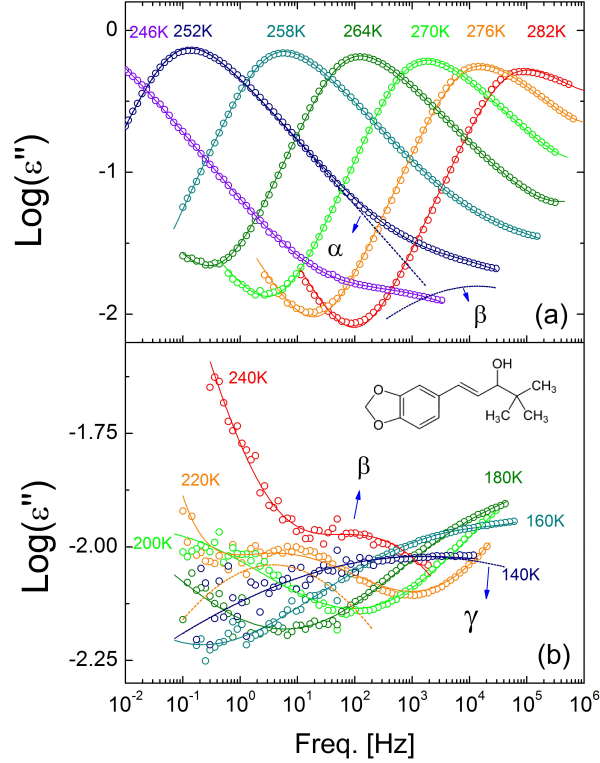
Figure 1: *(a)*: Loss spectra of STP measured between 246 and 282 K. Fits of α and β relaxations are displayed for the spectrum at 252 K. *(b)*: Loss spectra of STP measured between 140 and 240 K. Fits of β and γ relaxations can be seen in the measurements at 220 and 140 K, respectively. Inset: Molecular structure of STP.

The Arrhenius plot of the characteristic times (τ) corresponding to α, β and γ relaxations, as obtained from the fitting procedure, is shown in *Fig. 2*. The γ relaxation follows Arrhenius behavior with an activation energy $E_a = 23.5 \pm 0.1$ J/mol K. The β relaxation displays two different Arrhenius regimes with $E_a = 98.2 \pm 0.2$ J/mol K below T_g, and $E_a = 249 \pm 5$ J/mol K above T_g. The continuous line is the fit of τ_α using the Vogel-Fulcher-Tammann equation:[37]

$$\tau_\alpha = \tau_0 exp\left(\frac{D \cdot T_{VF}}{T - T_{VF}}\right) \qquad (3)$$

were the prefactor τ_0, the strength parameter D, and the Vogel - Fulcher temperature T_{VF} are phenomenological parameters with the following values obtained from the fit: $Log(\tau_0/(s)) = -16.2 \pm 0.3$, $D = 10.3 \pm 0.5$ and $T_{VF} = 198 \pm 1$ K. The horizontal dashed

line indicates the value of τ_α which is conventionally taken to mark the glass transition temperature ($Log(\tau_\alpha) = 2$, $i.e$ $\tau_\alpha = 100$ s). The intersection of the VFT fit and this dashed line gives a glass transition temperature of $T_g = 246.2 \pm 0.5$ K. The inset of *Fig. 2* (a) shows the calorimetry thermogram of STP, which was acquired upon heating from below T_g, after previously cooling the sample from the molten state at a rate of $2K/min$. The arrow indicates the onset T_g value obtained from the two tangents (dashed lines), which is 248 ± 1 K, in agreement with the data obtained from the BDS data and with the previously reported T_g value.[38]
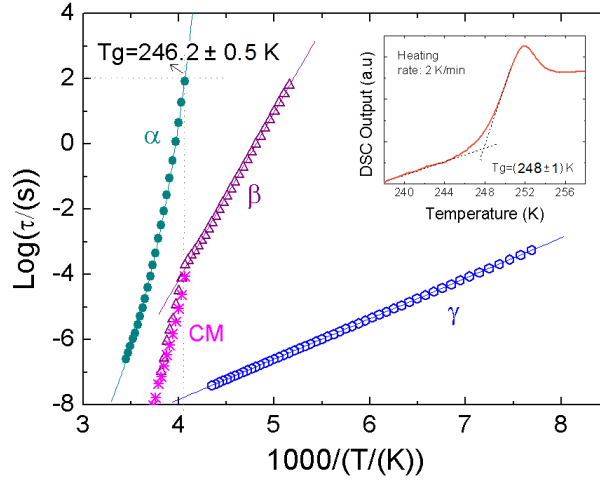

Figure 2: Arrhenius plot of the primary (α, filled green circles) and secondary (β, purple triangles and γ, blue empty circles) relaxation times, as extracted from the loss spectra displayed in *Fig.1*. The continuous green line is the fit of τ_α using the Vogel-Fulcher-Tammann equation (*Eq. 3*). The horizontal dashed line indicates the glass transition temperature. Pink asterisks portray the values obtained for τ_β using the Coupling model (see text).[39,40] Inset: Differential scanning calorimetry thermogram acquired upon heating from the glass. The arrow indicates the onset T_g value obtained from the two tangents shown with dashed lines.

In agreement with the VFT model, T_{VF} is lower than T_g. The VFT temperature dependence confirms that the slower (α) relaxation has a cooperative nature, which becomes more pronounced when approaching the glass transition, which is a typical feature of correlated glass forming systems.

We can obtain from *Eq. 3*, the kinetic fragility index, m, of STP can be found as follows:[41]

$$m = \frac{D}{Ln(10)} \frac{T_{VF}}{T_g} \left(1 - \frac{T_{VF}}{T_g} \right)^{-2} \tag{4}$$

The experimental value obtained for STP is $m = 93 \pm 7$, which indicates this drug is a fragile glass former.

The interpretation of secondary relaxations is not as straightforward as for the primary one; a secondary relaxation may relate either to intramolecular motions involving the displacement of polar side-groups, or else it may be a Johari-Goldstein relaxation. The latter type of process involves the whole molecule and can be interpreted as the single-molecule relaxation, precursor of the cooperative α-relaxation according to the Coupling model.[39,42–45] The change in Arrhenius temperature dependence of τ_β at T_g is a characteristic feature that indicates the β relaxation is a Johari-Goldstein process.[40] This is also confirmed by the validity of the Coupling Model according to which, the relaxation time τ_{CM} of the Johari-Goldstein relaxation should be related to that of the primary process τ_α as:

$$\tau_{CM} = t_c^p \tau_\alpha^{(1-p)} \tag{5}$$

Here t_c's typical value is $2 \cdot 10^{-12}$ s and represents a cross-over time determined by the intermolecular interaction and independent of temperature.[40,46] The parameter p is equal to $1 - \beta_{KWW}$, where β_{KWW} is the stretched exponent that describes the shape of the α-relaxation process in the time domain.[47] For the obtained shape parameters (a, b) of the HN function employed to fit the primary relaxation, the following relation holds:[48,49] $p \cong 1 - (a \cdot b)^{1/1.23}$. We have calculated the corresponding time τ_{CM} with *Eq. 5* and plotted the results in the Arrhenius plot shown in *Fig. 2* (pink asterisks). The calculated Coupling Model values are virtually identical to the experimental ones. Hence, the β relaxation can be considered the precursor of the α process and it is a whole-molecule process. Consequently, the observed γ process must be an intramolecular process, linked to the dynamics of a subpart or side-group

of the non-rigid STP molecule.

Crystallization kinetics

In order to characterize the crystallization process from the supercooled liquid state into the stable crystalline state, we performed experiments at five fixed temperatures (T_e) above T_g, namely: 273.0, 275.5, 278.0, 283.0 and 293.0 K ($\pm$ 0.1) K. The decrease of $\Delta\epsilon$ over time (at a fixed temperature) is a quantitative measure of the amorphous fraction of the sample and thus of the kinetics of the (isothermal) recrystallization process, since the number of molecules participating in the cooperative α relaxation is proportional to the dielectric strength $\Delta\epsilon$.[50] During crystal growth, in fact, some molecules are removed from the supercooled liquid phase (where they are mobile), and form crystallites (where all motion stops). As an example, *Fig. 3* shows the real *(a)* and imaginary *(b)* part of complex dielectric permittivity, ϵ' and ϵ'' respectively, recorded at T_e=278.0 K in consecutive spectra (one every 190 seconds, approximately) during crystallization. The arrows indicate the spectral changes as crystallization progresses.
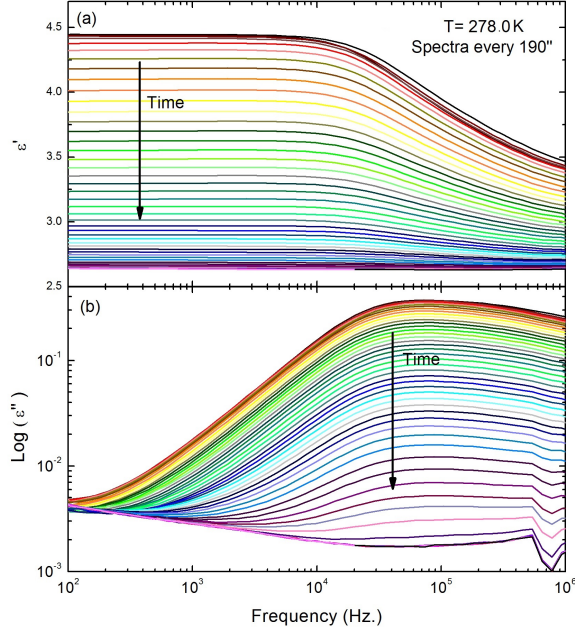
Figure 3: Spectra of the real *(a)* and imaginary *(b)* part of complex dielectric permittivity, ϵ' and ϵ'' respectively, recorded at T_e=278.0 K every 190 seconds during crystallization. The arrows indicate the evolution in time as crystallization progresses.

It can be observed that the recrystallization process produces a decrease in the intensity of the α relaxation peak, in the imaginary part of the dielectric permittivity, and correspondingly a decrease of static permittivity ϵ_s, and thus of the dielectric strength in the real part. *Fig. 4* shows the values of ϵ_s at 100 Hz, during isothermal crystallization at $T_e = 278.0$ K. The plateau at long times indicates full crystallization of the sample. The inset to *Fig. 4* shows a zoom-in at short times, where the intersection of two tangents marks the crystallization onset at time t_o. In each series of isothermal spectra, the static permittivity was taken to be the value of the real permittivity at a fixed frequency varying between 10^2 and 10^4 Hz depending on the measuring temperature, but always representing the low-frequency plateau value of the real permittivity.
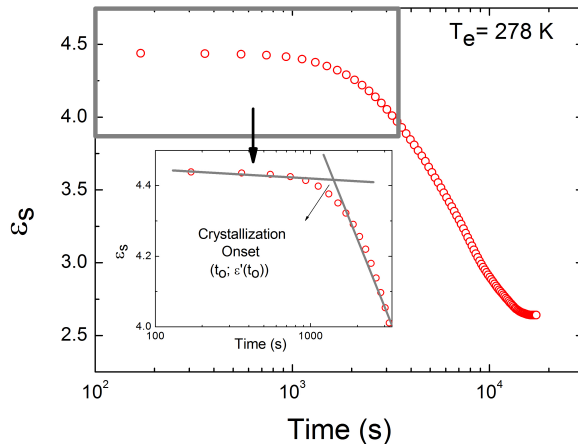
Figure 4: Evolution of the real static permittivity, ϵ_s, at 100 Hz as a function of time, for the data of Fig. 3 at $T_e = 278.0K$. The inset shows a zoom-in at short experiment times, where the intersection of the two gray lines marks the crystallization onset.

To analyze the crystallization kinetics of STP, we have studied the time evolution of the normalized static-permittivity difference, as defined by *D'Amore et al.*:[51]

$$\hat{\epsilon} = \frac{\epsilon_s(SL) - \epsilon_s(t)}{\epsilon_s(SL) - \epsilon_s(C)}. \tag{6}$$

Here, $\epsilon_s(SL)$ and $\epsilon_s(C)$ are the static permittivity of the supercooled liquid and the crystalline phase, respectively. The first value can be obtained by extracting ϵ_s at time zero (right after supercooling), and the second by doing the same thing at the end of the crystallization process, where the sample is completely crystalline and no further change is observed in ϵ_s (See *Fig.4*). $\epsilon_s(t)$ is the static permittivity of the mixed-phase sample as a function of the time elapsed from the start of the isothermal measurements. *Fig. 5* shows the $\hat{\epsilon}$ values obtained for all five experiments as a function of time. At short times $\hat{\epsilon} = 0$, since the sample is mainly in the supercooled state and the numerator vanishes. As the sample crystallizes, the value of $\epsilon_s(t)$ decreases approaching $\epsilon_s(C)$, until complete crystallization when $\hat{\epsilon}$ becomes unity.

In order to find a possible correlation between the relaxation time of the α relaxation and the characteristic crystal growth time of STP we have determined a characteristic crys-
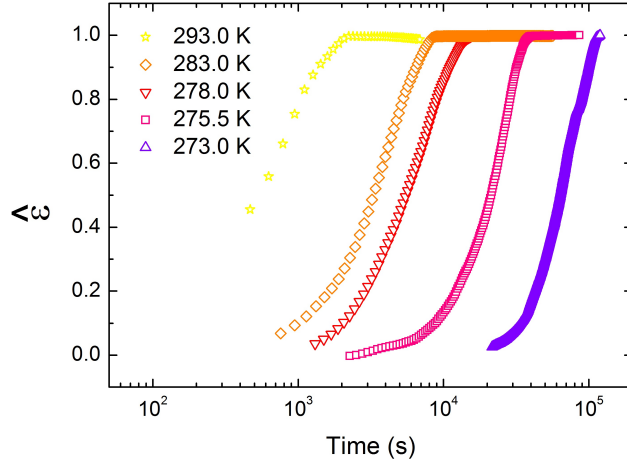
13

Figure 5: Time evolution of the normalized static-permittivity difference $\hat{\epsilon}$ during crystallization, as a function of the time elapsed since crystallization onset of each isothermal measurement (logarithmic scale) Stars, diamonds, inverted triangles, squares and triangles represent temperatures 293.0, 283.0, 278.0, 275.5 and 273.0 K respectively.

tallization time (t_c), as the time interval between the crystallization onset (t_o) and the time at which $\hat{\epsilon}$ becomes 0.25. In *Fig. 6* we plot the obtained t_c values as a function of the relaxation time of the cooperative dynamics, in logarithmic scale. For comparison, we also display similar data obtained from the literature[31] for the drugs celecoxib and indomethacin. There is a clear correlation between the two times in all cases. A linear regression gives for STP a slope value of (0.86 ± 0.07), whereas that reported for indomethacin and celecoxib is 0.8 ± 0.1. Interestingly, the experimental range of the slopes overlap, suggesting a possible universal slope value, at least above T_g. Nevertheless, further substances should be studied to be able to postulate a possible general model that could predict t_c for a given τ_α. It is also interesting to note that the dependence of t_c on τ_α is sublinear.

If the temporal dependence of the crystallization were Avrami-like,[52,53] then the normalized static-permittivity difference would follow:[54]

$$\hat{\epsilon}(t) = 1 - exp(-K(t - t_0)^n) \tag{7}$$

where K is the temperature-dependent crystallization rate and n is the Avrami exponent, which should be a constant that depends exclusively on the crystalline morphology and
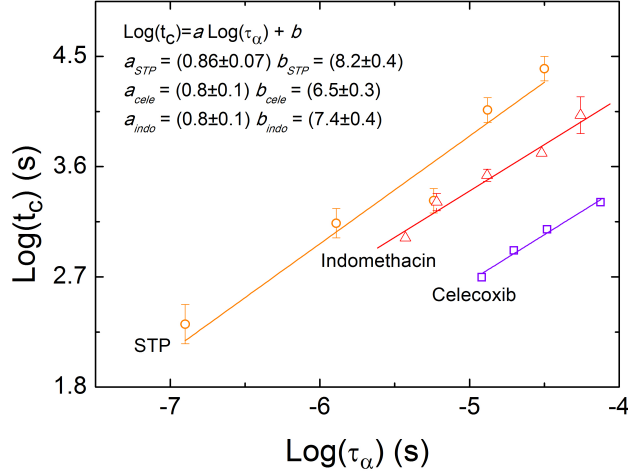
14

Figure 6: Plots of characteristic crystallization time (t_c) versus average α relaxation time above T_g in STP (circles), indomethacin (triangles) and celecoxib (squares). Values for indomethacin and celecoxib were obtained from reference.[31] Error bars are provided when n = 3; otherwise, the crystallization time is the average of two determinations.

crystallization mechanism.[55] *Fig. 7(a)* displays the Avrami plot at all studied temperatures. The normalized static-permittivity difference $\hat{\epsilon}$ is shown as a function of the time elapsed from the crystallization onset $(t - t_o)$ for each crystallization temperature. The inset shows the Arrhenius plot of the onset time, t_o. If the Avrami law were obeyed, each isothermal curve should look like a straight line, with constant slope equal to n. However, this is clearly not the case in *Fig. 7(a)*. To better visualize this fact, in *Fig. 7(b)* we have plotted the value of the effective (time-dependent) Avrami exponent for the temperature at which crystallization is slowest (namely, 273.0 K), defined as:

$$n = \frac{d(Ln(-Ln(1 - \epsilon')))}{d(Ln(t - t_o))} \tag{8}$$

As It is evident form *Fig. 7(b)* that the Avrami exponent is far from constant. In order to unambiguously state that the Avrami's law is not followed by this compound the errors affecting the data have been calculated using a block average technique. As it can be seen in Fig. 7 the variation of the curve is greater than the calculated errors, supporting again that Avrami's law is not followed. The inset in the same figure shows a curve obtained

by the subtraction of a linear curve to the experimental one in order to investigate if the exponent is constant or not in the most straightforward way. Again, the points seem not to follow an Avrami law, taking into account the obtained errors. Finally we have investigated if a different choice of t_o could be possibly causing the variations on the Avrami exponent. However t_o is only affecting an horizontal and vertical displacement of the curve of *Fig. 7(b)* and, thus, it cannot cause a deviation from linearity in *Fig. 7(b)*. At higher isothermal crystallization temperature, the effective Avrami coefficient is observed to vary between 1 and 2 (not shown). A value in this range would suggest a one-dimensional crystallization of STP into needle-like crystallites,[56] which is however not observed (see below). It is worth pointing out that similar departures from the Avrami law have been observed also in other compounds.[57]

To understand the reason underlying the failure of the Avrami law we performed diffraction experiments and observations of the crystallization process with an optical microscope. One possible cause of failure of the Avrami law, could be the existence of different polymorphs of STP, leading to the formation of crystallites with distinct structures and morphology, for example, as it happens for many pharmaceutical compounds.[58–63] This possibility is discarded by our X-ray diffraction measurements. *Fig. 8* shows the diffractograms obtained at (300 ± 1) K on the as-stored crystalline material, at (273 ± 1) K right after quenching from liquid state and at (300 ± 1) K after reheating.

It can be observed that the initial and recrystallized material display the same structure, and that the supercooled sample is indeed of glassy nature, as evidenced by the broad amorphous background. Within this broad feature, some crystalline Bragg reflections can be observed at $2\theta = 6, 15.6, 15.9, 18.8$ and 19.1. These correspond to the presence of a fraction of crystalline material. This behavior coincides with that observed by optical microscopy on molten drops at ambient temperature: while some drops recrystallized within approximately 10 minutes, some others remained liquid for much longer times. *Fig. 9* shows of the crystallization of pure STP as observed with an optical microscope.
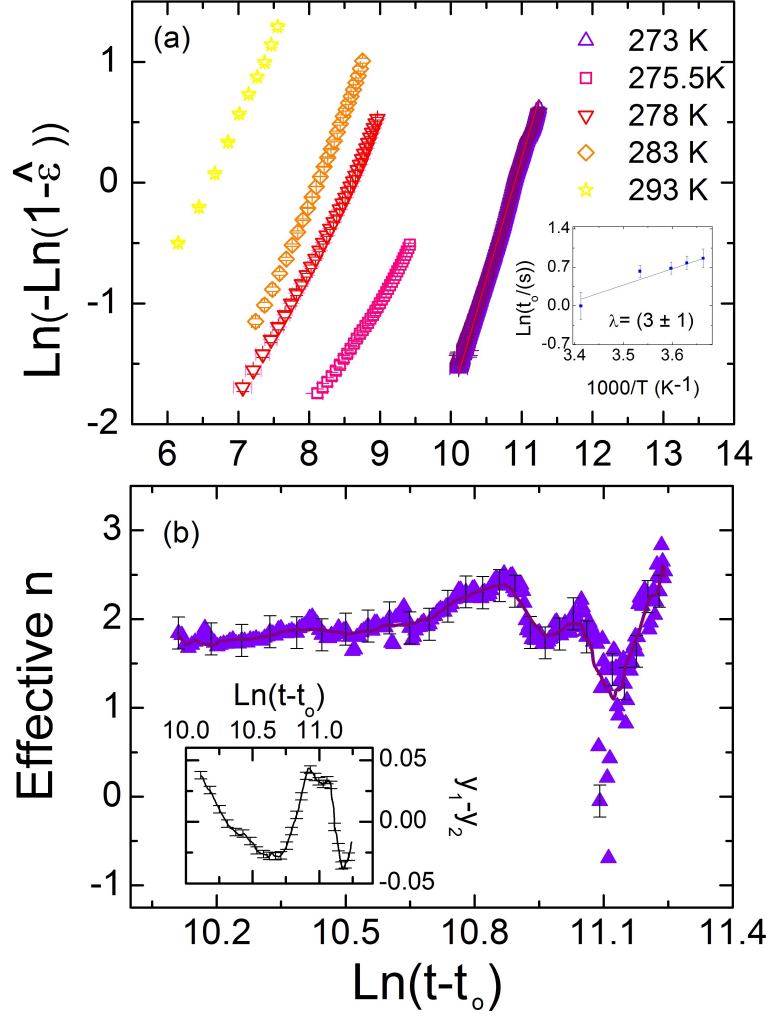
Figure 7: *(a)* Avrami plot of the normalized static-permittivity difference $\hat{\epsilon}$ as a function of the time elapsed from the crystallization onset $(t - t_o)$, for all five isothermal crystallization temperatures studied. Inset: Arrhenius plot of the onset time t_o. *(b)* Effective Avrami exponent *(Eq. (8))*, as a function of the time elapsed from the crystallization onset, for the measuring temperature of 273.0 K. Inset: Curve obtained by the subtraction of a linear curve to the experimental one.
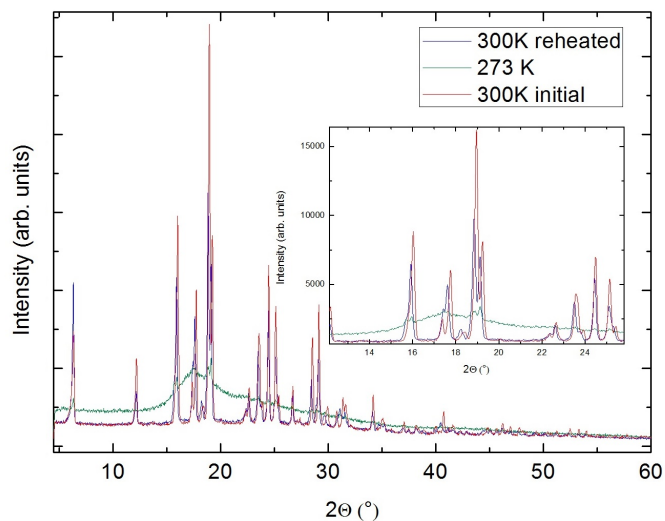
Figure 8: X-ray diffraction pattern of the as received STP powder at 300 K (blue), super-cooled liquid at 273 K (green) and recrystallized sample at 300 K (red). Inset: Zoom-in of the data at low scattering angles.
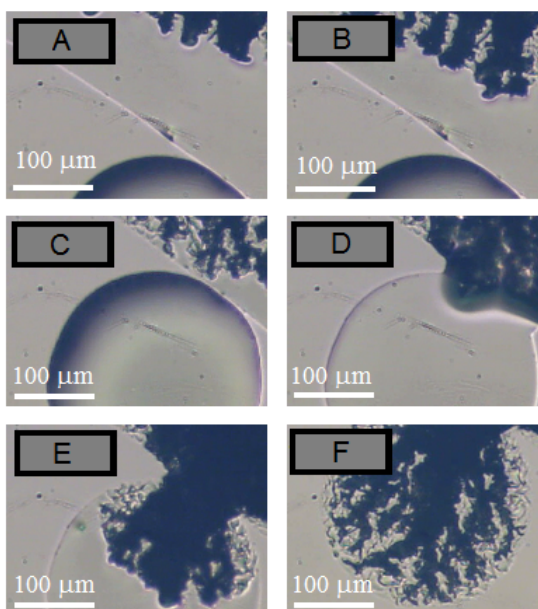

Figure 9: Crystallization of STP observed through an optical microscope with back-light illumination.

In the first photograph two regions can be clearly distinguished: a circular drop on the bottom and a bigger liquid domain on top, whose boundary is signaled by a white line. The dark region on the top right corner is the part of STP that is already crystalline. As time advances the growth of the crystal is observed. It can be noted in the first three photographs that the process is not unidirectional but rather results in a fractal 3D-morphology. Moreover, no other nucleation site appears in the liquid portion, apart from the first crystal. In other words, it is hard for STP crystals to nucleate, so that recrystallization generally proceeds from a single point (seed) towards the rest of the available liquid in all possible directions. This is evident also in the center and lower panels of *Fig. 9*, where a circular drop of liquid STP is visible. Such drop only starts to crystallize when crystallization of the larger liquid domain is complete. In picture D the growing crystal reaches the boundary with the single drop breaking its surface. As soon as the liquid of the second drop comes in contact with the crystal, it produces a burst of further crystal growth. In E the remaining part of the smaller drop is half crystallized and at F the process is complete. Black regions indicate higher crystalline structures, which are out of focus with respect to the height of the original liquid. It can be then affirmed that the crystalline phase grows as a function of the shape and size of the domains of the supercooled liquid, and that nucleation is the limiting step for crystallization. This, together with the fractal-like crystal growth, helps rationalizing why the Avrami theory is not fully satisfied. The Avrami exponent can in fact change during crystallization if the growth morphology changes.[64]

Conclusions

By studying Stiripentol (STP) in its supercooled liquid and glass state, three different relaxations were identified: the α relaxation peak, corresponding to the collective reorientation of the STP molecules, a Johari Goldstein β relaxation that is the precursor of the α process according to the Coupling model, and a γ relaxation which corresponds to an intramolecu-

lar relaxation. The T_g of the material was determined both by dielectric spectroscopy and calorimetry, obtaining $T_g = 246.2 \pm 0.5$ K and $T_g = 248 \pm 1$ K, respectively.

Isothermal crystallization of STP was studied at temperatures between 273.0 and 293.0 K. It is found that the Avrami law is not obeyed. This happens because STP has difficulties when nucleating, and possibly also because the crystalline phase grows in a fractal 3D morphology. It appears that supercooled liquid STP requires in general relatively high temperatures to produce a crystalline nucleus, from which crystal growth proceeds so fast, that no other nucleation site is generated during crystallization of a given liquid domain. As observed by means of X-ray diffraction, the initial solid and the recrystallized material display the same structure, which indicates that no other polymorph of STP appears at ambient pressure. A sublinear correlation is found between the characteristic crystal-growth time and the collective relaxation dynamics. This correlation was observed also in other substances, and suggests a general correlation at temperatures above T_g to predict a substance's crystallization time as a function of temperature. Further materials should be studied so as to test this possibility.

Acknowledgement

References

(1) Vasconcelos, T.; Sarmento, B.; Costa, P. Solid dispersions as strategy to improve oral bioavailability of poor water soluble drugs. *Drug Discovery Today* **2007**, *12*, 1068–1075.

(2) Ikegami, K.; Tagawa, K.; Osawa, T. Bioavailability and in Vivo Release Behav-

ior of Controlled-Release Multiple-Unit Theophylline Dosage Forms in Beagle Dogs, Cynomolgus Monkeys, and Göttingen Minipigs. *J. Pharm. Sci.* **2006**, *95*, 1888–1895.

(3) Rathbone, M.; Hadgraft, J.; Roberts, M. *Modified-release drug delivery technology*; New York: Marcel Dekker, 2003.

(4) Bhardwaj, S.; Arora, K.; Kwong, E.; Templeton, A.; Clas, S.; Suryanarayanan, R. Correlation between Molecular Mobility and Physical Stability of Amorphous Itraconazole. *Mol. Pharmaceutics* **2013**, *10*, 694–700.

(5) Zhou, D.; Zhang, G.; Law, D.; Grant, D.; Schmitt, E. Physical stability of amorphous pharmaceuticals: Importance of configurational thermodynamic quantities and molecular mobility. *J. Pharm. Sci* **2002**, *91*, 1863–1872.

(6) Gupta, P.; Chawla, G.; Bansal, A. Physical Stability and Solubility Advantage from Amorphous Celecoxib: The Role of Thermodynamic Quantities and Molecular Mobility. *Mol. Pharmaceutics* **2004**, *1*, 406–413.

(7) Serajuddin, A. Solid dispersion of poorly water-soluble drugs: Early promises, subsequent problems, and recent breakthroughs. *J. Pharm. Sci.* **1999**, *88*, 1058–1066.

(8) B.C. Hancock, M. P. What is the true solubility advantage for amorphous pharmaceuticals? *Pharm. Res.* **2000**, *17*, 397–404.

(9) Craig, D.; Royall, P.; Kett, V.; Hoptopn, M. The relevance of the amorphous state to pharmaceutical dosage forms: glassy drugs and freeze dried systems. *Int. J. Pharm.* **1999**, *179*, 179–207.

(10) Kaminski, K.; Kaminska, E.; Adrjanowicz, K.; Grzybowiska, K.; Wlodarczyk, P.; Paluch, M.; Burian, A.; Ziolo, J.; Lepek, P.; Mazgalski, J.; Sawicki, W. Dielectric relaxation study on tramadol monohydrate and its hydrochloride salt. *J. Pharm. Sci.* **2010**, *99*, 94–106.

(11) Yin, S.; Franchini, M.; Chen, J.; Hsieh, A.; Jen, S.; Lee, T.; Hussain, M.; Smith, R. Bioavailability enhancement of a COX-2 inhibitor, BMS-347070, from a nanocrystalline dispersion prepared by spray-drying. *J. Pharm. Sci.* **2005**, *94*, 1598–1607.

(12) Qian, F.; Tao, J.; Desikan, S.; Hussain, M.; Smith, R. Mechanistic Investigation of Pluronic® Based Nano-crystalline Drug-polymer Solid Dispersions. *Pharm. Res.* **2007**, *24*, 1551–1560.

(13) Wu, T.; Yu, L. Surface Crystallization of Indomethacin Below T_g. *Pharm. Res.* **2006**, *23*, 2350–2355.

(14) Patterson, J.; James, M.; Forster, A.; Lancaster, R.; Butler, J.; Rades, T. The influence of thermal and mechanical preparative techniques on the amorphous state of four poorly soluble compounds. *J. Pharm. Sci.* **2005**, *94*, 1998–2012.

(15) Yu, L. Amorphous pharmaceutical solids: preparation, characterization and stabilization. *Adv. Drug Deliv. Rev.* **2001**, *48*, 27–42.

(16) Aso, Y.; Yoshioka, S.; Kojima, S. Relationship Between the Crystallization Rates of Amorphous Nifedipine, Phenobarbital, and Flopropione, and Their Molecular Mobility as Measured by Their Enthalpy Relaxation and ^{1}H NMR Relaxation Times. *J. Pharm. Sci.* **2000**, *89*, 408–416.

(17) Hancock, B.; Shamblin, S.; Zografi, G. Molecular mobility of amorphous pharmaceutical solids below their glass transition temperatures. *Pharm. Res.* **1995**, *12*, 799–806.

(18) Andronis, V.; Zografi, G. The molecular mobility of supercooled amorphous indomethacin as a function of temperature and relative humidity. *Pharm. Res.* **1998**, *15*, 835–842.

(19) Yoshioka, S.; Aso, Y. A quantitative assessment of the significance of molecular mobility

as a determinant for the stability of lyophilized insulin formulations. *Pharm. Res.* **2005**, *22*, 1358–1364.

(20) Alie, J.; Menegotto, J.; Cardon, P.; Duplaa, H.; Caron, A.; Lacabanne, C.; Bauer, M. Dielectric study of the molecular mobility and the isothermal crystallization kinetics of an amorphous pharmaceutical drug substance. *J. Pharm. Sci.* **2004**, *93*, 218–233.

(21) Kolodziejczyk, K.; Paluch, M.; Grzybowska, K.; Grzybowski, A.; Wojnarowska, Z.; Hawelek, L.; Ziolo, J. Relaxation dynamics and crystallization study of sildenafil in the liquid and glassy states. *Mol. Pharm.* **2013**, *10*, 2270–82.

(22) Wojnarowska, Z.; Grzybowska, K.; Hawelek, L.; Dulski, M.; Wrzalik, R.; Gruszka, I.; Paluch, M.; Pienkowska, K.; Sawicki, W.; Bujak, P.; Paluch, K.; Tajber, L.; Markowski, J. Molecular dynamics, physical stability and solubility advantage from amorphous indapamide drug. *Mol. Pharm.* **2013**, *10*, 3612.

(23) Graesera, K.; Patterson, J.; Zeitler, J.; Gordon, K.; Rades, T. Correlating thermodynamic and kinetic parameters with amorphous stability. *European J. of Pham. Sci.* **2009**, *37*, 492–498.

(24) Grzybowska, K.; Capaccioli, S.; Paluch, M. Recent developments in the experimental investigations of relaxations in pharmaceuticals by dielectric techniques at ambient and elevated pressure. *Adv. Drug Del. Rev.* **2016**, *100*, 158–182.

(25) Trojnar, M.; Wojtal, K.; Trojnar, M.; Czuczwar, S. Stiripentol. A novel antiepileptic drug. *Pharmacol. Rep.* **2005**, *57*, 154–160.

(26) Wirrell, E.; Laux, L.; Franz, D.; Sullivan, J.; Saneto, R.; Morse, R.; Devinsky, O.; Chugani, H.; Hernandez, A.; Hamiwka, L.; Mikati, M.; Valencia, I.; Guern, M. L.; Chancharme, L.; de Menezes, M. S. Stiripentol in Dravet syndrome: results of a retrospective U.S. study. *Epilepsia* **2013**, *54*, 1595–1604.

(27) Stiripentol, BCX 2600. *Drugs in R &D* **2002**, *3*, 220–222.

(28) Afifi, S. Solid Dispersion Approach Improving Dissolution Rate of Stiripentol: a Novel Antiepileptic Drug. *Iranian J. Pharm. Research* **2015**, *14*, 1001–1014.

(29) Bebin, M.; Bleck, T. New anticonvulsant drugs. Focus on flunarizine, fosphenytoin, midazolam and stiripentol. *Drugs* **1994**, *48*, 153–171.

(30) Sada, N.; Lee, S.; Katsu, T.; Otsuki, T.; Inoue, T. Epilepsy treatment. Targeting LDH enzymes with a stiripentol analog to treat epilepsy. *Science* **2015**, *347*, 1362–1367.

(31) Mehta, M.; Ragoonanan, V.; McKenna, G. B.; Suryanarayanan, R. Correlation between Molecular Mobility and Physical Stability in Pharmaceutical Glasses. *Mol. Pharm.* **2016**, *13*, 1267–1277.

(32) Johari, G.; Kim, S.; Shanker, R. Dielectric Relaxation and Crystallization of Ultraviscous Melt and Glassy States of Aspirin, Ibuprofen, Progesterone, and Quinidine. *J. Pharm. Sci.* **2007**, *96*, 1159–1175.

(33) Larini, L.; Ottochian, A.; Michele, C. D.; Leporini, D. Universal scaling between structural relaxation and vibrational dynamics in glass-forming liquids and polymers. *Nature Phys.* **2008**, *4*, 42–45.

(34) Bhugra, C.; Shmeis, R.; Krill, S.; Pikal, M. Different measures of molecular mobility: comparison between calorimetric and thermally stimulated current relaxation times below Tg and correlation with dielectric relaxation times above Tg. *J. Pharm. Sci.* **2008**, *97*, 4498–515.

(35) Havriliak, S.; Negami, S. A complex plane analysis of α-dispersions in some polymer systems. *J. Polym. Sci.* **1966**, *16*, 99–117.

(36) Havriliak, S.; Negami, S. A complex plane representation of dielectric and mechanical relaxation processes in some polymers. *Polymer* **1967**, *8*, 161–210.

(37) Angell, C. Structural instability and relaxation in liquid and glassy phases near the fragile liquid limit. *J. Non-Cryst. Solids* **1988**, *102*, 205–221.

(38) Céolin, R.; Dugué, J.; Rouland, J.; Ralambosoa, C.; Lepage, F. Solid state studies on stiripentol: a novel anticonvulsant drug. *Int. J. Pharm.* **1991**, *74*, 77–82.

(39) Ngai, K. Relation between some secondary relaxations and the α relaxations in glass-forming materials according to the coupling model. *J. Chem. Phys.* **1998**, *109*, 6982–6994.

(40) Ngai, K. Why the glass transition problem remains unsolved? *J. Non-Cryst. Solids* **2007**, *353*, 709–718.

(41) Böhmer, R.; Ngai, K.; Angell, C.; Plazek, D. Nonexponential relaxations in strong and fragile glass formers. *J. Chem. Phys.* **1993**, *99*, 4201–4209.

(42) Ngai, K.; Paluch, M. Classification of secondary relaxation in glass-formers based on dynamic properties. *J. Chem. Phys.* **2004**, *120*, 857–873.

(43) Ngai, K. *Relaxation and Diffusion in Complex Systems*; Springer: New York, 2011.

(44) Capaccioli, S.; Paluch, M.; Prevosto, D.; Wang, L.-M.; Ngai, K. Many-Body Nature of Relaxation Processes in Glass-Forming Systems. *J. Phys. Chem. Lett.* **2012**, *3*, 735–743.

(45) Ngai, K. An Extended Coupling Model Description of the Evolution of Dynamics with Time in Supercooled Liquids and Ionic Conductors. *J. Phys. Condens. Matter* **2003**, *15*, S1107–S1125.

(46) Colmenero, J.; Arbe, A.; Coddens, G.; Frick, B.; Mijangos, C.; Reinecke, H. Crossover from Independent to Cooperative Segmental Dynamics in Polymers: Experimental Realization in Poly(Vinyl Chloride). *Phys. Rev. Lett.* **1997**, *78*, 1928–1931.

(47) Kohlrausch, R. Theorie des elektrischen Rückstandes in der Leidener Flasche. *Ann. Phys. Chem. (Poggendorff)* **1854**, *56*, 91.

(48) Alvarez, F.; Alegra, A.; Colmenero, J. Relationship between the time-domain Kohlrausch-Williams-Watts and frequency-domain Havriliak-Negami relaxation functions. *Phys. Rev. B* **1991**, *44*, 7306–7312.

(49) Alvarez, F.; Alegría, A.; Colmenero, J. Interconnection between frequency-domain Havriliak-Negami and time-domain Kohlrausch-Williams-Watts relaxation functions. *Phys. Rev. B* **1993**, *47*, 125–130.

(50) Kremer, F.; Schönhals, A. *Broad Band Dielectric Spectroscopy. Ch. 3 and 4.*; Springer: Berlin.

(51) D'Amore, A.; Kenny, J.; Nicolais, L.; Tucci, V. Dynamic-mechanical and dielectric characterization of PEEK crystallization. *Polym. Eng. Sci.* **1990**, *30*, 314–320.

(52) Avrami, M. Kinetics of Phase Change. I General Theory. *J. Chem. Phys.* **1939**, *7*, 1103–1112.

(53) Avrami, M. Kinetics of Phase Change. II Transformation - Time Relations for Random Distribution of Nuclei. *J. Chem. Phys.* **1940**, *8*, 212–224.

(54) Adrjanowicz, K.; Kaminski, K.; Wojnarowska, Z.; Dulski, M.; Hawelek, L.; Pawlus, S.; Paluch, M. Dielectric Relaxation and Crystallization Kinetics of Ibuprofen at Ambient and Elevated Pressure. *J. Phys. Chem. B* **2010**, *114*, 6579–6593.

(55) Wunderlich, B. *Macromolecular Physics. Crystal Nucleation, Growth, Annealing, Vol. 2.*; Academic Press: London, 1976.

(56) Tripathi, P.; Romanini, M.; Tamarit, J.; Macovez, R. Collective relaxation dynamics and crystallization kinetics of the amorphous Biclotymol antiseptic. *Int. J. Pharm.* **2015**, *495*, 420–427.

(57) Sanz, A.; Niss, K. Coupling between Molecular Mobility and Kinetics of Crystal Growth in a Hydrogen-Bonded Liquid. *Cryst. Growth Des.* **2017**,

(58) Espeau, P.; Céolin, R.; Tamarit, J. L.; Perrin, M.; Gauchi, J.; Leveiller, F. Polymorphism of paracetamol: relative stabilities of the monoclinic and orthorhombic phases inferred from topological pressure-temperature and temperature-volume phase diagrams. *J. Pharm. Sci.* **2005**, *94*, 524.

(59) Barrio, M.; Espeau, P.; Tamarit, J.; Perrin, M.; Veglio, N.; Céolin, R. Polymorphism of progesterone: relative stabilities of the orthorhombic phases I and II inferred from topological and experimental pressure-temperature phase diagrams. *J. Pharm. Sci.* **2009**, *98*, 1657.

(60) Barrio, M.; Maccaroni, E.; Rietveld, I.; Malpezzi, L.; Masciocchi, N.; Céolin, R.; Tamarit, J. Pressure - Temperature State Diagram for the Phase Relationships Between Benfluorex Hydrochloride Forms I and II: A Case of Enantiotropic Behavior. *J. Pharm. Sci.* **2012**, *101*, 1073.

(61) Toscani, S.; Céolin, R.; Minassian, L. T.; Barrio, M.; Veglio, N.; Tamarit, J.; Louer, D.; Rietveld, I. Stability hierarchy between Piracetam forms I, II, and III from experimental pressure-temperature diagrams and topological inferences. *Int. J. Pharm.* **2016**, *497*, 96.

(62) Céolin, R.; Tamarit, J.; Barrio, M.; López, D.; Nicolai, B.; Veglio, N.; Perrin, M.; Espeau, P. Overall monotropic behavior of a metastable phase of biclotymol, 2,2 '-methylenebis(4-chloro-3-methyl-isopropylphenol), inferred from experimental and topological construction of the related P-T state diagram. *J. Pharm. Sci.* **2008**, *97*, 3927.

(63) Gana, I.; Barrio, M.; Ghaddar, C.; Nicolai, B.; Do, B.; Tamarit, J.; Safta, F.; Rietveld, I. An integrated view of the influence of temperature, pressure, and humidity on the stability of trimorphic cysteamine hydrochloride. *Mol. Pharm.* **2015**, *12*, 2276.

(64) Jensen, M.; Alba-Simionesco, C.; Niss, K.; Hecksher, T. A systematic study of the

isothermal crystallization of the mono-alcohol n-butanol monitored by dielectric spectroscopy. *J. Chem. Phys.* **2015**, *143*, 134501.

Graphical TOC Entry